Article │ Received 14 January 2025; Accepted 25 April 2025; Published 20 June 2025
https://doi.org/10.55092/sc20250014

Multi-dimensional data interpretation for defective filter identification

Pengkun Liu[1], Jinghua Xiao[2] and Pingbo Tang[1,*]

[1] Department of Civil and Environmental Engineering, Carnegie Mellon University, Pittsburgh, PA 15213, USA
[2] Circular Water Solution, LLC, Bryn Mawr, PA 19010, USA

* Correspondence author; E-mail: ptang@andrew.cmu.edu.

Highlights:

- Developed a non-invasive approach with 3D and sensor data to identify defective water filters.
- Demonstrated surface irregularities correlate with subsurface imperfections and sensor readings.

Abstract: Inspecting water filters in treatment facilities is tedious and costly, often requiring manual media disruption, significant labor, and extended downtime. These challenges underscore the need for improved methods to assess filter conditions efficiently and accurately. Given the essential role of water filters in safeguarding water infrastructure, periodic evaluations are crucial to detecting irregularities, such as unevenness or misalignment in the gravel support layers and piping within the filter system. Such structural anomalies can disrupt water flow across filtration layers, compromising water quality standards due to inadequate backwash operations characterized by unregulated, high-speed water streams from the filter base aimed at cleansing the filter media. Traditional inspection techniques, which require physically disturbing the filter media, are time-consuming and labor-intensive, involving at least two personnel for several hours, and risk overlooking defects due to limited sampling areas. To address these challenges, this study examines a new non-invasive approach that leverages the uneven backwash process and water flow data to identify water filters that contain defective filtration materials and structural problems without contact-based inspection. A central hypothesis of our investigation is that when subsurface structural irregularities disrupt normal backwash operations and flow patterns, they subsequently produce both visible surface deformations and distinctive anomalies in recorded sensor data. This non-invasive method assesses filters' structural health and backwash efficiency in water treatment facilities through 3D laser scanning and sequential sensor data analysis. It aims to streamline the inspection process and reduce the costs and inaccuracies associated with manual media interruption. The results show uneven geometric features of the filter medium surface correlated with underlying structural faults and filter performance degradation, which is also validated by the sensor data. The proposed method offers a comprehensive understanding of the condition of water filters.

Keywords: water treatment plant; filter diagnosis; point cloud; time series analysis

1. Introduction

Water filters are critical components in water treatment plants (WTPs), serving as the last physical barrier to remove suspended solids and pathogens [1]. Ensuring their structural integrity and proper functioning is essential for effective water treatment and public health protection [2]. However, inspecting water filters remains challenging and costly, often requiring labor-intensive methods involving media disruption, extended downtime, and the risk of overlooking defects. Current inspection methods for water filters rely on the probe rod technique to monitor the surface of the underlying gravel layer or the excavation method to expose the sub-drain system for visual inspection [3]. Additionally, interpreting results requires experienced operators, which can be challenging during personnel turnover. These challenges underscore the importance of developing efficient and accurate inspection methods to assess filter conditions and maintain optimal performance. Consequently, specialists in water management are pursuing alternative non-invasive techniques that can precisely and dependably evaluate aggregate interfaces and drainage infrastructure without requiring destructive intervention.

The filtration process represents a crucial phase in water purification systems, tasked with extracting particulate matter to ensure turbidity measurements remain under 0.3 NTU following chemical preprocessing and gravitational separation of substantial particulates [3]. When unforeseen malfunctions develop within filtration mechanisms, the effluent may fail to meet the required standards. In conventional surface water treatment plants, filter servers are the last physical barrier to removing suspended solids and pathogens. Therefore, maintaining the structural integrity of the filter and executing appropriate backwash procedures are critical for effective treatment and safeguarding the community.

Researchers and engineers have considered using 3D imaging and related technology for non-invasive inspections to reduce time, costs, and errors associated with conventional water infrastructure inspections. For example, monitoring 3D geometric changes of the filtration layers' top surface could reveal uneven changes caused by uneven gravel support beneath. Furthermore, monitoring changes in relative distances and angles between the filtration media surface and nearby filter elements (e.g., wash-water troughs) could indicate uneven settlements underneath. 3D imaging technology can support accurate and detailed geometric assessments of exposed filter structures and filtration media surfaces to predict subsurface geometric defects. Nevertheless, owing to insufficient three-dimensional analytical records and the absence of established relationships between geometric changes and hidden defects, only seasoned professionals are capable of accurately associating surface pattern variations with specific underlying problems and defective regions.

Therefore, this research proposes establishing automatic spatial change pattern recognition and time series analysis methods that leverage high-resolution dimensional mapping of filtration surfaces and water filter sensor data to identify and interpret anomalous geometric change patterns correlated with underlying geometric defects and backwash problems. Such a method would not require water filter inspectors to perform laborious field punches to discover geometric defects related to the backwash of structures buried under the top filtration layers. The hypothesis for this paper is that irregular backwash procedures and water flows caused by underlying structural defects could produce non-uniform three-dimensional topographical alterations on the top surface and abnormal sensor data.

The research questions and associated challenges are as follows:

(1) What 3D geometric changes on the top surface of filtration layers can reveal uneven geometric changes caused by defective interior structures?

(2) Can 3D geometric changes and sensor data patterns reveal and interpret uneven backwash processes?

The objectives of this study are: (1) Derive geometric changes in the exposed structures of the water filters and the surface of the filtration media through field 3D laser scanning before and after inspections of six water filters. We collect 3D images for six water filters that will be inspected with conventional methods or planned for capital improvements. The 3D image data collection (3D laser scanning) will be before and after the inspection or capital improvements that allow direct observations. A deviation analysis algorithm developed by the research team for the diagnosis of structure deformation will then compare 3D images before and after inspection to derive 3D geometric change patterns; (2) Identify and interpret the abnormal filters with underlying geometric defects and backwash problems through the exposed surface of the filtration layers and sensor data from the water treatment plant.

The subsequent sections are organized as follows: Section 2 defines the motivation case. Section 3 reviews the literature. Section 4 delineates the proposed framework with multimodal data interpretation for defective filter identification. Section 5 describes the experimental results and discussions. Section 6 concludes with comments and directions for future research.

2. Motivating case

Figure 1 shows the internal structure filtration layers of a multimedia water filter, including anthracite, sand, support graves, and underdrains. Conventional drinking water treatment plants incorporate multiple sequential elements and associated mechanisms: coagulation-flocculation, sedimentation, filtration, and disinfection [4]. Throughout normal functioning, preliminarily processed water descends vertically through the purification apparatus, enabling the porous substrate to intercept and retain suspended particulates. Subsequently, the substructure collection network gathers the clarified liquid. Periodically, water from the underdrain is backwashed to the top to clean the filtration media. The underdrain system supports the gravel and filter media while distributing the backwash water. A defective filter system can result in ineffective backwashing, creating “dead zones” that often lead to turbidity exceedances and violations of treatment standards. Routine filter system inspection is crucial for early problem detection, preventing costly repairs of damaged or malfunctioning filter components.

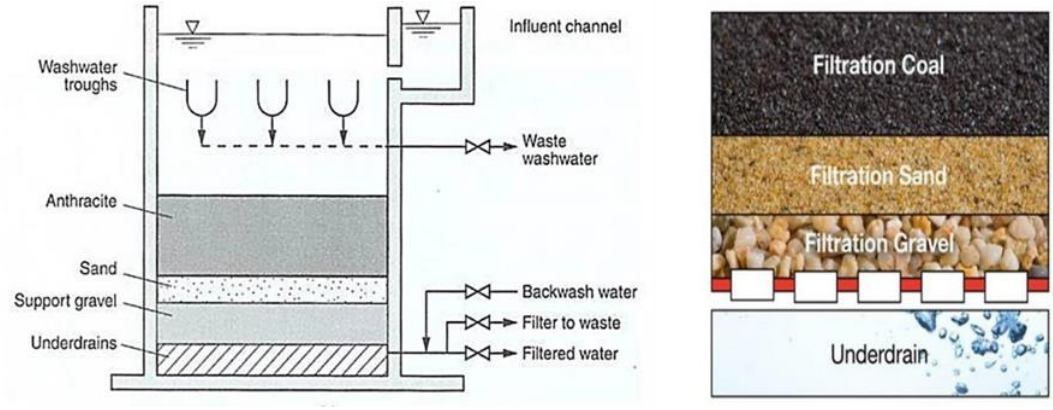

Figure 1. Illustration of the internal structure of the filtration layers of a water filter.

Between 2003 and 2013, failures in the traditional water industry continued to occur frequently in developed countries, leading to drinking water outbreaks caused by microbial contamination due to infrastructure failures [5]. For example, in the spring of 2001, a cryptosporidiosis outbreak occurred in North Battleford, Saskatchewan, Canada. This outbreak was caused by the sedimentation contact unit's inadequate removal of suspended solids from the source water, resulting in a filter breakthrough. Consequently, thousands of people became ill, with approximately 50 individuals hospitalized [6].

Filtration is a critical component of the water treatment process, responsible for removing suspended solids and microorganisms such as Cryptosporidium oocysts and Giardia cysts [3]. Drinking water regulations strictly mandate that the concentrations of Giardia cysts and Cryptosporidium oocysts remain within specified limits to ensure water safety. However, Cryptosporidium is resistant to standard disinfection practices like chlorination, making filtration essential for its removal from drinking water. Several studies have demonstrated that reducing the turbidity of filtered water from 0.3 NTU to 0.1 NTU can effectively remove cysts.

Proper backwashing is crucial for the effective maintenance of a filter. As depicted in Figures 2(a) and 2(b), uniform water flow results in an even medium surface after draining. In contrast, improper backwashing, as shown in Figures 2(c) and 2(d), leads to uneven surfaces after draining despite uniform water flow. Improper backwashing can cause media loss, media mixing, and the formation of mud balls, cracks, and craters, all of which contribute to inadequate filtration and increased effluent turbidity.

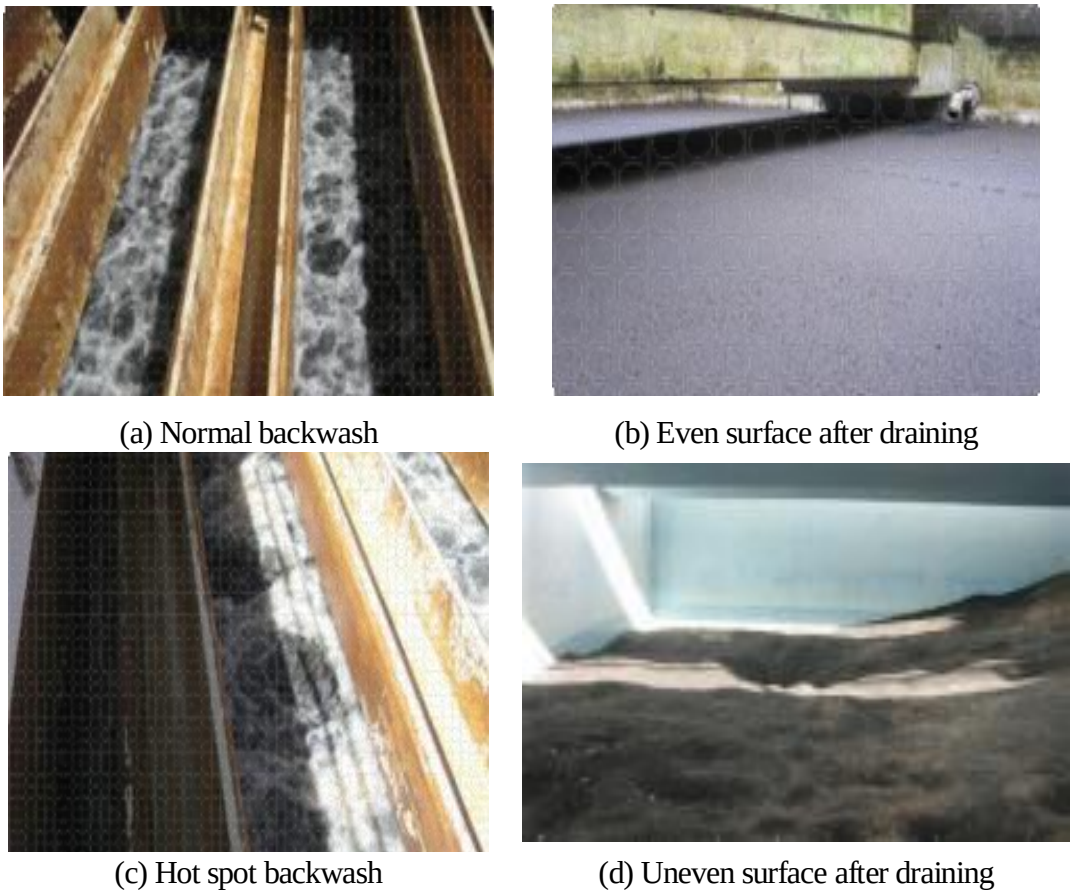

(a) Normal backwash (b) Even surface after draining

(c) Hot spot backwash (d) Uneven surface after draining

Figure 2. Backwash and medium surface [7] (Reprinted with permission. Copyright (2014), Laurel Passantino and Jacqueline Rhoades).

Consequently, scheduled examination of filtration systems proves crucial for identifying emerging issues promptly and avoiding expensive remediation of deteriorated or improperly functioning filtration elements. Traditional assessment approaches, such as the probe rod or excavation method, require field sampling of layer shapes and depths to map the 3D configuration of buried gravel layers and identify integrity issues with backwash pipes. Such evaluation techniques prove disruptive and labor-intensive, necessitate service suspensions, introduce potential hazards, and depend heavily upon operators' assessments and practical knowledge, potentially introducing interpretive prejudices into analytical conclusions.

3. Literature review

A thorough understanding of existing research and methodologies is essential for advancing WTP filtration systems' inspection and fault diagnosis. This Literature Review synthesizes current practices in WTP filtration inspection, explores innovative infrastructure inspection techniques utilizing laser point cloud data, examines the role of time series analysis in fault diagnosis, and identifies critical research gaps that necessitate further investigation. By evaluating these areas, this review provides a foundation for the proposed study's objectives and methodologies.

3.1. Current water treatment plant filtration inspection

Consistent turbidity levels below 0.3 NTU characterize effective filter performance, particle counts under 50 particles/mL, filters operating continuously for more than 24 hours, and minimal premature particle breakthrough [4]. Several methods are employed to assess filter performance, including the filter rise rate test, backwash water turbidity profiling, bed expansion tests, visual backwash observations, media depth and gravel mapping, media sampling and testing, and floc retention analysis.

The gravel support bed comprises various layers of gravel of different sizes and coarse sand above the underdrain network in a granular filter. This configuration ensures the even distribution of backwash water throughout the filter and supports the filtration media on the surface. A properly designed, constructed, and maintained filter should have a level gravel support bed. When the gravel support bed is level, backwash water is evenly distributed, preventing the formation of dead zones—areas with little to no flow or mixing—during the backwashing process. However, improper backwashing procedures or deviations from proper protocols can result in an uneven gravel support bed.

Evaluations of hydraulic filtration units typically depend on the probe rod method to monitor the surface of the underlying gravel layer or the excavation method to expose the sub-drain system for visual inspection [8]. These methods involve determining measurement points based on specific sampling patterns, such as grids defined in inspection manuals. Inspectors assess the media depth at these points to evaluate the filter bed's conditions, including the levelness of the gravel support and the integrity of backwash pipes.

Figure 3(a) illustrates the fluidized bed method, where the inspector selects a measurement point and drops a punch plate into the fluidized filtration sand. Backwashing continues until the plate contacts the gravel surface, and the depth reading at this location is recorded. Multiple depth measurements at sampled points capture the 3D shape of the gravel support surface, allowing for the calculation of levelness and flatness. The second method, depicted in Figure 3(b), utilizes an excavation box to punch

through fluidized filtration sand to measure depths. These methods require extensive fieldwork and can take hours to complete depth measurements. The third method, shown in Figure 3(c), employs a punch rod instead of a plate to measure depths at sampled points. While rods can penetrate dry filtration sand without needing a fluidized bed and ongoing backwashing, the depth accuracy is lower than punch plates. Additionally, prolonged measurements only produce sparse depth samples, possibly overlooking structural anomalies situated in the intervals between measurement locations. In summary, conventional water filter inspection requires intensive on-site dimensional assessment of filtration substrates and frequently fails to detect spatial irregularities that compromise cleansing operations and performance outcomes.

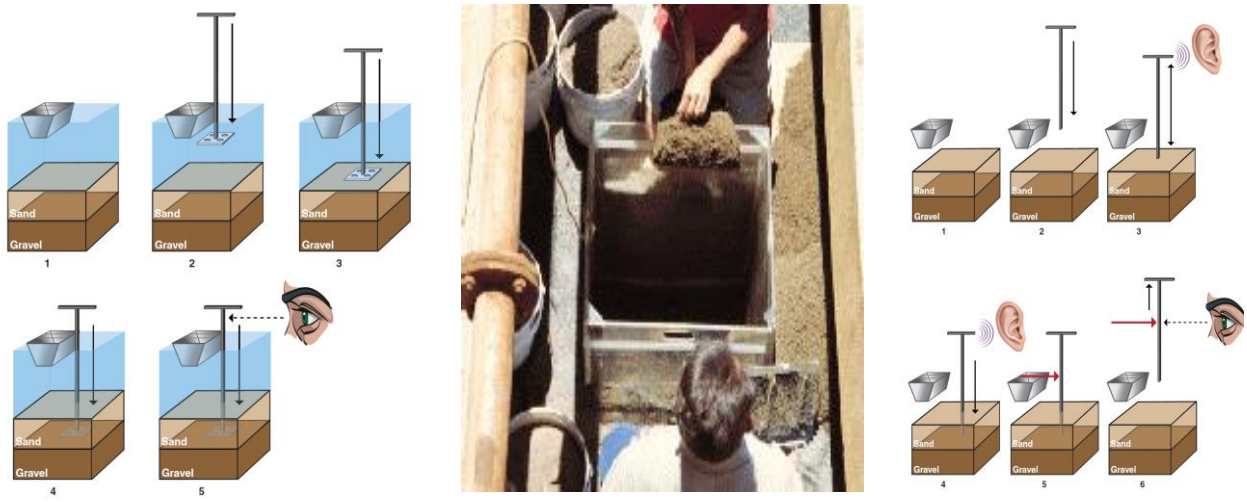

(a) Fluidized bed method (b) Illustration of the excavation box method (c) Punch-rod method

Figure 3. Current water treatment plant filtering inspection [3].

3.2. Infrastructure inspection based on laser point cloud

Extensive research has been conducted on using 3D point cloud data obtained from laser scanners for fast, accurate, and non-invasive infrastructure inspection [9]. Bosché and Guenet [10] segmented the acquired point clouds on site with the corresponding BIM model to obtain the standard straight edge and F numbers. The proposed approach was tested and validated on two actual concrete slabs. Puri *et al.* [11] combined terrestrial laser scanning with the continuous wavelet transform to control surface flatness. This method provided accurate and dense data sets and performed high-resolution frequency analysis in the spatial and frequency domains. The results of the tests on the two real concrete floors outperformed the Waviness Index method. Wang *et al.* [12] proposed using laser scanning technology for inspection of the surface flatness and distortion of pre-cast concrete elements and estimated three measurements: warping, bowing, and differential elevation between adjacent elements. Liu *et al.* [13] used terrestrial laser scanners for the quality inspection of multiple pre-cast concrete elements simultaneously to improve inspection efficiency. In particular, to extract the different types of precast concrete elements from the point clouds, a segmentation and recognition approach was proposed. Li *et al.* [14] developed a practical and general approach to assessing the flatness quality of concrete surfaces with color-coded deviation maps. A constructed room and two full-scale pre-cast concrete components were used to validate the proposed method.

Especially for the inspection of the infrastructure system of the water industry, Erdélyi *et al.* [15] documented the application of ground-based laser measurement technology to track structural alterations in aeration tanks at water processing facilities. Yu *et al.* [16] developed an integrated approach combining dimensional scanning with thermal radiation visualization to identify fluid escape points by simultaneously capturing both spatial configuration and characteristic properties of hydraulic failures. Moritani *et al.* [17] proposed a point cloud registration and model fitting method based on cylinders by terrestrial laser scanners for the water treatment plant piping system, considering the scanner parameters and cylinder parameters to avoid propagation of registration errors and modeling errors. Marzouk *et al.* [18] established a methodological structure employing volumetric laser measurement to acquire maintenance-relevant data supporting building information modeling applications through the categorical organization of equipment details from water processing installations. Yang *et al.* [19] fused the RGB 2D image, the temperature information, and the 3D point cloud to detect defects to improve the reliability of the power equipment and reduce the work pressure of the operation and maintenance personnel. Chethana *et al.* [20] developed an optimized graphical representation component for virtual modification planning alongside a systematic lattice-based hydraulic movement simulation approach to enhance strategic planning for pipeline renovation projects. Catalin *et al.* [21] used a workflow methodology that compares the 3D mesh acquired using photogrammetry techniques with an accurate terrestrial laser scan applied to the pipe design of the water treatment plant. However, these studies primarily focus on dimensional or flatness measurements of on-site objects, lacking a comprehensive diagnosis of the underlying causes of fault situations.

3.3. Time series analysis for interpretation fault diagnosis

Numerous investigators have implemented sequential data examination techniques for anomaly identification within water management systems. As an illustration, Faruk developed an integrated approach combining ARIMA methodology with artificial neural networks for chronological data forecasting, analyzing 108 monthly recordings of aquatic quality parameters—such as thermal measurements, boron concentrations, and oxygen saturation levels—collected between 1996 and 2004 from the Büyük Menderes River in Turkey [22]. Liu *et al.* proposed a time series proton exchange membrane fuel cell water failure diagnosis method based on the bidirectional long- and short-term memory network and t-distributed stochastic neighbor [23]. Liu *et al.* proposed a hybrid water quality monitoring device fault diagnosis model based on multiclass support vector machines and rule-based decision trees [24]. Li *et al.* proposed a novel adversarial generative network-based anomaly detection method with LSTM-RNN to capture the distribution of multivariate time series of sensors and actuators for complex cyber-physical systems [25]. Wang *et al.* proposed a sensor and actuator fault diagnosis method for small pressurized water reactors using extended short-term memory networks to learn features from multivariable time series data and capture long-term dependencies with a labeled fault dictionary established to map complex fault modes [26].

Furthermore, various investigators have developed analytical frameworks for malfunction identification through information processing. Ghoneim established an innovative methodology for analyzing gaseous compounds in solution, utilizing 386 distinct samples to resolve conventional analytical discrepancies in transformer malfunction categorization [27]. Chen *et al.* formulated a malfunction detection and explanation approach incorporating probabilistic neural computational

structures alongside structured definition protocols to overcome the difficulty of understanding the fault diagnosis decision process [28]. Liu *et al.* developed a systematic approach for anomaly identification and diagnostic insight generation by grouping parameters around underlying factors and implementing relationship-based categorization techniques for architectural energy management infrastructures [29]. However, the diagnosis and interpretation of time series faults specifically for water treatment filters remain underexplored due to the invisibility and concealment of the filter medium. There is a lack of research focused on explaining abnormal sensor data in this context. Our approach uniquely combines time series signal analysis with 3D geometric surface data, establishing direct correlations between operational anomalies detected in temporal patterns and physical irregularities in filter media structure, thereby providing both detection capability and explanatory power that traditional single-domain methods cannot achieve.

3.4. Research gaps

The review of related studies reveals three primary knowledge gaps in water treatment plant filter inspection and diagnosis: (1) Existing inspection methods are invasive, time-consuming, cause operational interruptions, raise safety concerns, and rely on operators' subjective judgment and experience, which may bias data interpretation. The current probe rod technique and excavation method require field sampling of layer shapes and depths to map the 3D configuration of buried gravel layers and identify integrity issues with backwash pipes. There is a lack of non-invasive inspection methods to detect defective filters without physical disruptions. (2) Due to the invisibility of the filter medium and the complexity of the water treatment plants' filters, identifying the underlying causes of abnormal filter performance is challenging. Integrating sensor data with geometrical data could facilitate mutual interpretation to understand gravel surface and under-drain conditions of filters. (3) There is a scarcity of comprehensive datasets documenting geometric information, sensor data, and other relevant information necessary for effective filter fault detection. The lack of datasets integrating geometric and time-series signals limits AI's ability to learn meaningful patterns, leading to biased models and unreliable fault detection. This scarcity necessitates manual intervention by human experts to interpret data and define rules, which is time-intensive and hinders scalability. Addressing this gap is critical for advancing data-driven, non-invasive inspection methods central to this research. To address these issues, this research aims to explore and analyze whether uneven backwash processes caused by irregular gravel support or defective backwash pipes can produce uneven 3D geometric changes on the top surface and abnormal sensor data.

4. The proposed framework with multi-modal data interpretation for defective filter identification

This research introduces a comprehensive framework integrating geometric information from 3D point clouds with time-series sensor data to inspect and analyze water filters during backwash operations, as shown in Figure 4. High-resolution 3D laser scanning is utilized to capture the geometric changes on the exposed media surfaces of the filters before and after the backwash process. Key geometric features such as roughness, mean curvature, Gaussian curvature, omnivariance, and planarity are computed to detect surface irregularities, as discussed in Sections 4.1 and 5.1. Advanced clustering methods are applied to classify the geometric features and isolate normal and abnormal filter conditions. In parallel, sensor data,

including turbidity, backwash frequency, and flow rate, are analyzed to identify abnormal operational patterns such as frequent backwashing, elevated turbidity levels, and reduced water production, as discussed in Sections 4.2 and 5.2. Integrating these multi-modal data sources—geometric changes and sensor-based time-series analysis—enables a holistic assessment of filter performance. Defective filters are identified through collective interpretation of these data modalities, validated by CFD (computational fluid dynamics) simulations for enhanced accuracy and reliability (Section 5.3).

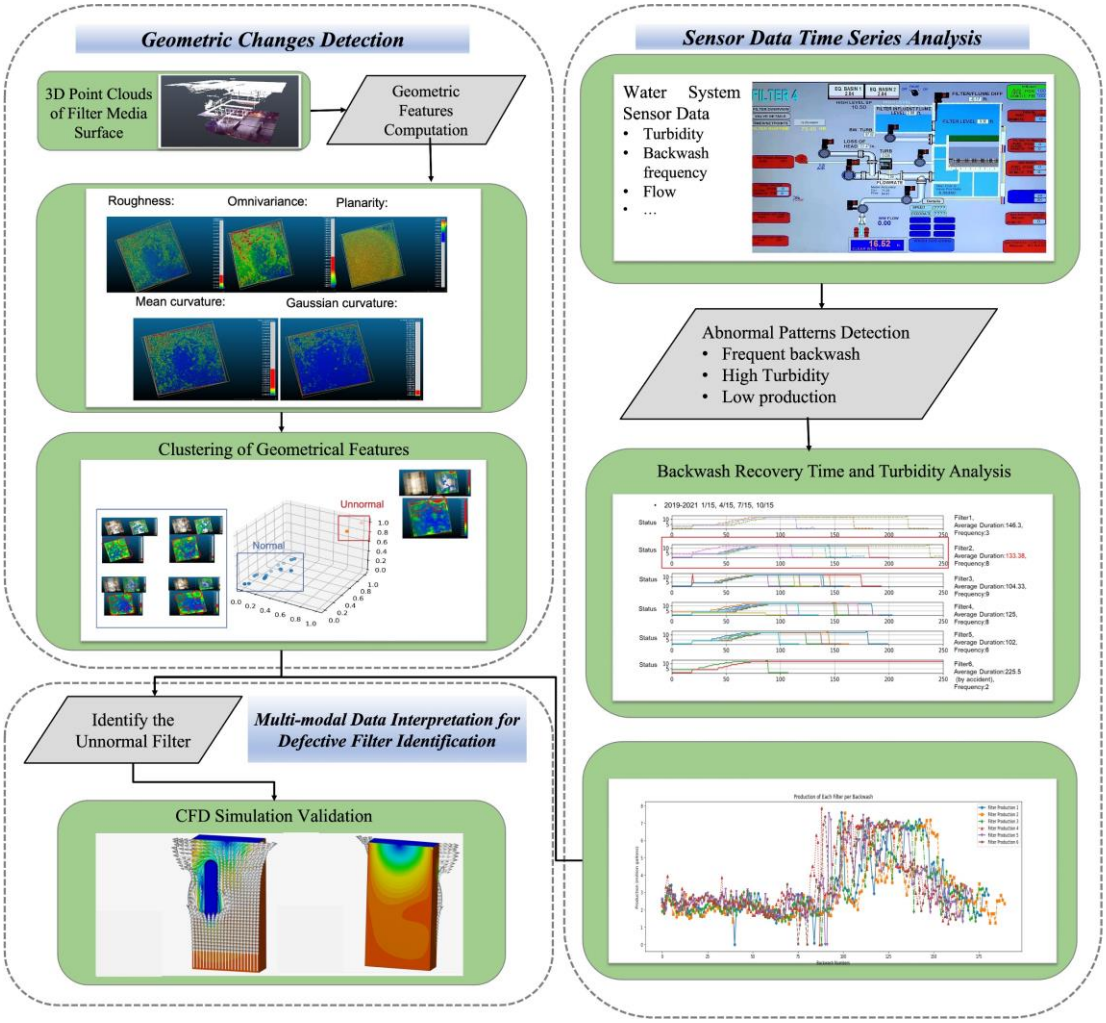

Figure 4. The proposed multi-modal data interpretation framework for the identification of defective filters.

4.1. Water filter media surface point cloud collection and geometrical change analysis

4.1.1. Water filter media surface point cloud collection

As depicted in Figures 5(a) and 5(b), the water filter is a rectangular tank installed underground. To scan the surface of the water filter media, an upside-down laser scanner is installed, enabling the collection of 3D point cloud data representing the geometric information of the filter surface, as shown in Figures 5(c) and 5(d). Before backwashing, the water filter medium appears brown and dirty (Figure 6(a)). The subsequent steps—backwash air scouring, filter boiling, and filter-to-waste—are

carried out in sequence (Figures 6(b) and 6(c)). Thereafter, the water filter medium is restored to a gray, clean state (Figure 6(d)).

(a) Top of the water filter

(b) Upside-down installation of the laser scanner

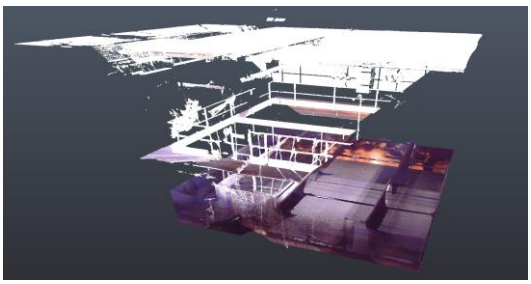

(c) 3D points cloud data of the water filter

(d) The surface of the water filter

Figure 5. Water filter media surface point cloud dataset collection.

(a) The surface of the water filter medium before backwash

(b) Backwash air wash and filter boils

(c) Filter-to-waste backwash

(d) The surface of the water filter medium after backwash

Figure 6. The processes of the water filter backwash.

After nine years, the six-filter medium will be replaced with a new medium. Basically, workers would dig the medium and expose the underdrains to inspect whether the underdrains are blocked with sand or particles, as shown in Figure 7(a). At the same time, workers would clean the left gravel support bed materials in the underdrains. Figure 7(b) shows the materials from the drilled gravel support bed. After inspecting the underdrains, the water treatment plant operators would wash the underdrains without any medium to clean the underdrain systems, as shown in Figure 7(c).

(a) Underdrains inspection

(b) The gravel supports bed materials

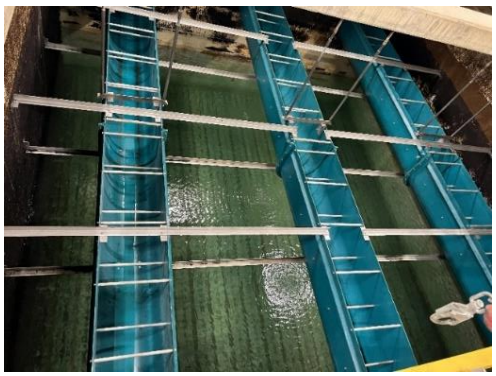

(c) Backwash of underdrain

Figure 7. Change of water filter medium and inspection of underdrain.

4.1.2. Water filter media surface point cloud geometrical change analysis

The surface of the medium should remain as level as possible in a properly designed, constructed, and maintained filter. However, during operation and backwashing, the medium can be dislodged by water flow, leading to an uneven surface. Improper backwashing procedures, such as the formation of mud balls, filter layer mixtures, or an uneven underlying gravel layer, can result in an uneven medium surface. Therefore, measuring the medium's depth and flatness can reflect the filter's functional status. The medium's depth is measured as the distance between the surface of the water filter medium and the ground floor (reference plane), as shown in Figure 8. Since all six filters share the same ground floor, the medium depth for each filter is obtained by comparing the distance between the media surface and the ground floor.

Furthermore, to find the typical geometric features to describe the characteristics between normal and unnormal water filters, we compare different geometric features, including the roughness, curvature (mean curvature, Gaussian curvature, and normal change rate), density (number of neighbors, surface

density, and volume density), moment (1st order moment), features (sum of eigenvalues, ominvariance, eigenentropy, anisotropy, planarity, linearity, surface variation, sphericity, verticality). Using these calculated geometric features, K-means clustering is applied to categorize filters as normal or abnormal in high-dimensional space.

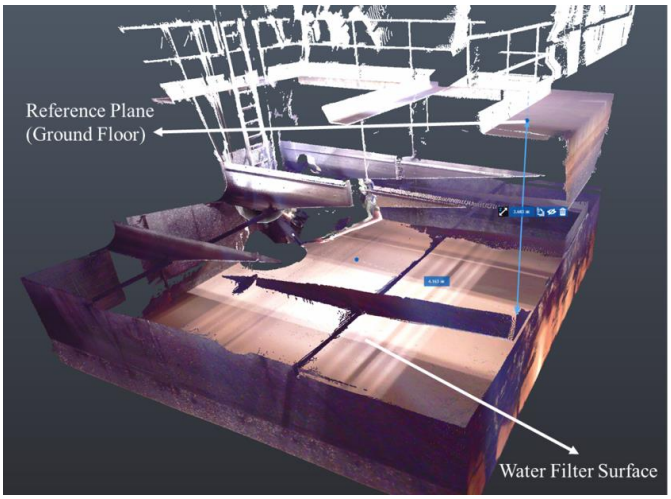

Figure 8. Water filter medium elevation analysis.

To obtain the eigenvalues of the point cloud, a 3D neighborhood is defined as a sphere centered on the search point [30]. Then, we could define the local neighbor m in the 3D point clouds through the matrix M [30]:

$$M = \begin{bmatrix} x_1 - \bar{x} & y_1 - \bar{y} & z_1 - \bar{z} \\ \vdots & \vdots & \vdots \\ x_m - \bar{x} & y_m - \bar{y} & z_m - \bar{z} \end{bmatrix} \quad (1)$$

Then, it is calculated for each 3D point and its respective 3D covariance matrix within the local neighborhood. From which a covariance matrix ($M^T M$) is derived as:

$$M^T M = \begin{bmatrix} \sum_{i=1}^{m} (x_i - \bar{x})^2 & \sum_{i=1}^{m} (x_i - \bar{x})(y_i - \bar{y}) & \sum_{i=1}^{m} (x_i - \bar{x})(z_i - \bar{z}) \\ \sum_{i=1}^{m} (x_i - \bar{x})(y_i - \bar{y}) & \sum_{i=1}^{m} (y_i - \bar{y})^2 & \sum_{i=1}^{m} (y_i - \bar{y})(z_i - \bar{z}) \\ \sum_{i=1}^{m} (x_i - \bar{x})(z_i - \bar{z}) & \sum_{i=1}^{m} (y_i - \bar{y})(z_i - \bar{z}) & \sum_{i=1}^{m} (z_i - \bar{z})^2 \end{bmatrix} \quad (2)$$

From this covariance matrix, the eigenvalues and eigenvectors are derived. The eigenvector corresponding to the shortest eigenvalue defines the fit normal of an orthogonal regression plane, and the centroid of the set of points defines a point on this plane. The derived eigenvalues λ_1, λ_2 *and* λ_3 of the covariance matrix could be utilized to define the geometric features describing the local 3D structure of the point clouds [31–33] as shown in Table 1. Sum of eigenvalues $\sum_\lambda$ describes the total variation, which is the sum of the squared distances of the points of a neighborhood from their centroid; Planarity P_λ measures the smoothness of the local neighborhood point cloud; Omnivariance O_λ describes how a neighborhood of points spread homogeneously across a 3D volume; Eigenentropy E_λ provides a measure of the order or disorder of 3D points within the covariance ellipsoid. Anisotropy A_λ measures the differences between each eigenvector. Linearity L_λ investigates whether a set of points can be modeled by a 3D line. Sphericity S_λ investigates the sphericity of a neighborhood 3D points. Curvature is the absolute value of the rate of change of the tangent line's angle of inclination relative to

the distance along the curve. Roughness for each point equals the distance between this point and the best-fitting plane computed on its nearest neighbors.

Table 1. Geometric features based on eigenvalues and eigenvectors of the structure tensor.

Summary of Geometric Features		
Sum of eigenvalues	$\sum_{\lambda} = \lambda_1 + \lambda_2 + \lambda_3$	(3)
Ommivariance	$O_\lambda = (\lambda_1 * \lambda_2 * \lambda_3)^{\frac{1}{3}}$	(4)
Planarity	$P_\lambda = \frac{\lambda_2 - \lambda_3}{\lambda_1}$	(5)
Eigenentropy	$E_\lambda = -\sum_{i=1}^{3} \lambda_i \ln(\lambda_i)$	(6)
Anisotropy	$A_\lambda = \frac{\lambda_1 - \lambda_3}{\lambda_1}$	(7)
Linearity	$L_\lambda = \frac{\lambda_1 - \lambda_2}{\lambda_1}$	(8)
Sphericity	$S_\lambda = \frac{\lambda_3}{\lambda_1}$	(9)
Change of curvature	$C_\lambda = \frac{\lambda_3}{\lambda_1 + \lambda_2 + \lambda_3}$	(10)

The geometric features (roughness, curvature, omnivariance, and planarity) were selected based on their ability to characterize structural anomalies caused by subsurface defects. These features are derived from eigenvalues of the point cloud covariance matrix (Equations (1) and (2)), which mathematically quantify spatial deviations in 3D geometry: Roughness measures local surface irregularity, reflecting disruptions from mud balls or gravel misalignment. Curvature (mean/Gaussian) captures bending energy, identifying abnormal deformations correlated with uneven backwash flow. Omnivariance evaluates the homogeneity of point distributions, detecting regions with displaced filter media. Planarity distinguishes flat *vs.* warped surfaces, which is critical for assessing gravel layer integrity. These features are universally applicable to granular media filters (anthracite, sand, *etc.*) as they focus on relative geometric changes rather than absolute material properties. However, operational thresholds may require calibration for specific filter designs (e.g., size, underdrain configurations) through baseline scans under normal conditions.

While the selected features are broadly generalizable, two safeguards ensure reliability: One is normalization: Elevation differences are measured relative to a fixed ground plane (Figure 8), decoupling material-specific roughness from defect-induced changes. The other is Adaptive Clustering: K-means clustering (Figure 14) identifies anomalies through deviation patterns rather than fixed thresholds, accommodating design variations. For example, anthracite's natural surface roughness (higher baseline roughness than sand) would not trigger false alarms, as anomalies are defined by relative changes post-backwash. This approach was validated across six filters with varying operational histories.

4.2. Sensor data time series analysis

We could evaluate the filters' performances through the time series sensor data. There are several criteria values for evaluating typical filter performances, such as such as filtered water turbidity, backwash times, water production, head loss, particle counts, filtration rate, filter input turbidity, backwash rate,

wash water turbidity at the end of the wash, shake test result, time to form clear patches during backwash, residual coagulant, and various additional criteria [34]. For example, the turbidity of filtered water greater than 1 NTU increases the potential of chlorine demand and bacteria shielding. Water production consists of two parts: the amount of water production between each backwash and the total water production in a limited time.

We obtain the sensor data from the SCADA system of the water treatment plant as shown in Figure 9, including (1) flow rate, (2) effluent turbidity, (3) loss of flow; (2) effluent turbidity, (3) loss of head, (4) backwash rates, (5) filter levels, (6) flume levels (filter influent flume level) and (7) filter status (13 assigned numbers for each status, as shown in Table 2).

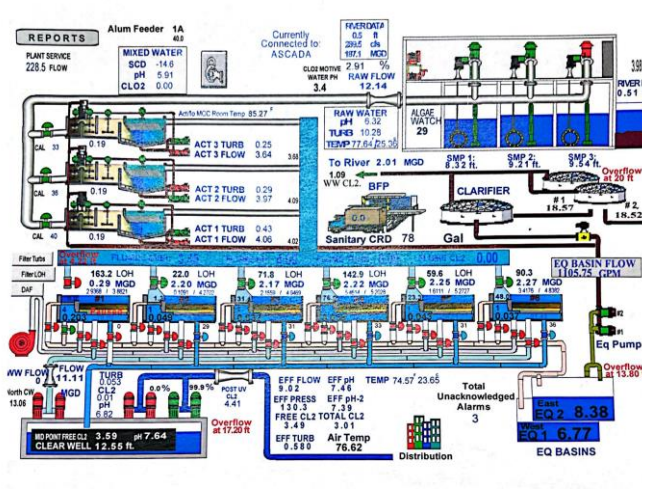

(a) The SCADA layout of the water treatment plant includes six filters

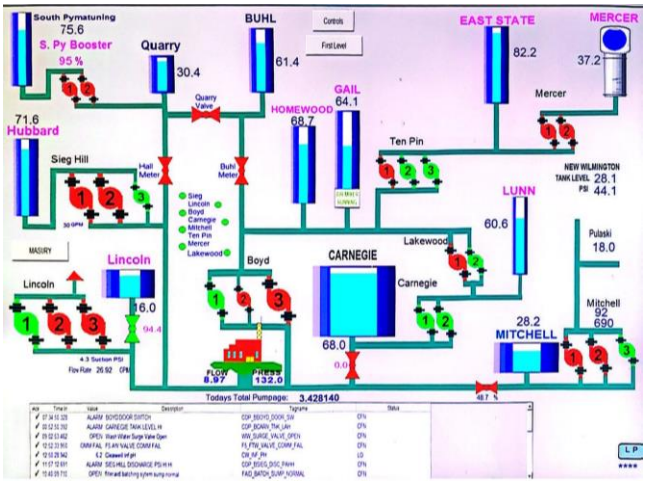

(b) The connections between the pumps and valves

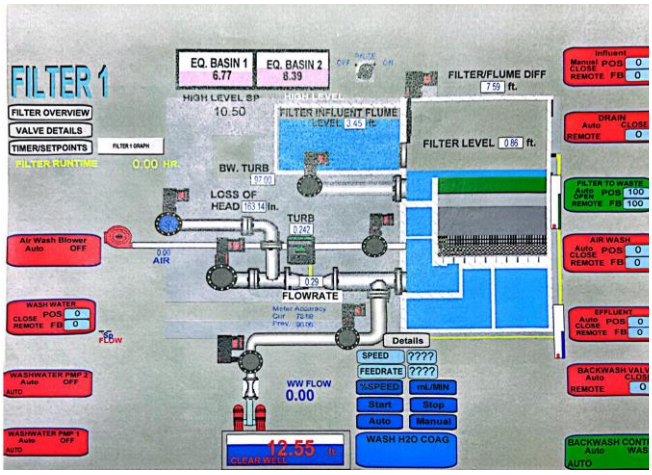

(c) The detailed control screen of the water filter

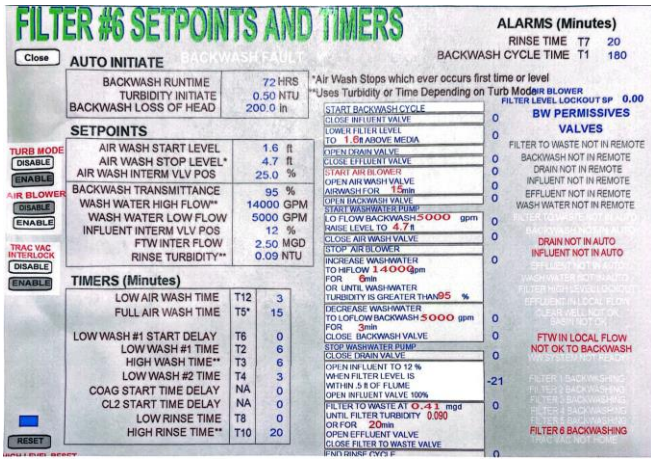

(d) Backwash setpoints and timers

Figure 9. SCADA system of the water treatment plant.

Table 2. The illustrations of filter states.

Numbers	Filter States
0	0-Out of Service
1	1-In Production
2	2-Production Pause
3	3-FTW (non-backwash)
4	4-BW Drawdown
5	5-BW Pause
6	6-BW Air Wash
7	7-BW AIR & Low Wash 1
8	8-Low Wash 1
9	9-BW High Wash
10	10-BW Low Wash 2
11	11-BW Refill
12	12-BW FTW
13	13-BW FTW & Production

Figure 10 illustrates the six backwash statuses and flow rates of the filters. The backwash of the filter consists of several steps. The filter needs to change to offline out of production. Then, the water is drained to a level above the surface of the medium. The compressed air wash flows up from the bottom underdrains through the filter medium to expand and separate the particles. After the air wash cycle is completed, the water flows up from the bottom and under the filter medium to carry the particles in suspension through the wash water. The duration of the backwash depends on the turbidity of the backwash water. When the turbidity of the backwash water is below the set point. In the AQUA water treatment plant, the detail backwash cycle includes (1) closing influent valve, (2) lower filter level to 1.6 ft above media, (3) opening the drain valve, (4) closing effluent valve, (5) lower filter level to 1.6 ft above media, (6) closing FTW valve, (7) open air wash valve to start air wash for 15 min, (8) open backwash valve, (9) controlling the flow backwash 5000 gpm to raise the level to 4.7 ft, (10) close air wash valve, (11) stop air blower, (12) increase wash water to high flow: 14000 gpm for 6 minutes or until wash water turbidity of wash water is greater than 98%, (13) decrease wash water to low flow backwash: 5000 gpm for 3 minutes, (14) close backwash valve, (15) stop wash water pump, (16) close drain valve, (17) open influent to 12%: when filter level is within 0.5 ft of the flume, open influent valve 100%, (18) filter to waste: at 0.3 mgd until filter turbidity 0.090 or for 20 minutes, open effluent valve.

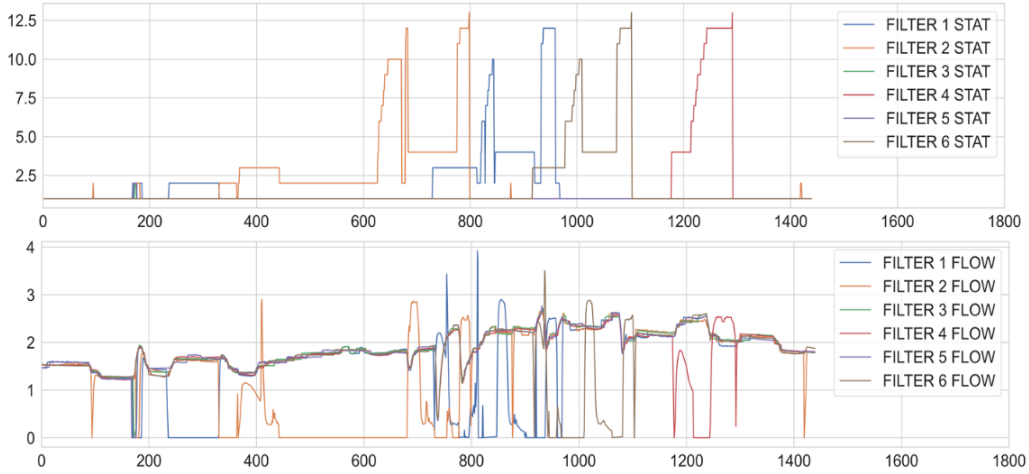

Figure10. Illustration of six filter backwash status and flow rate.

5. Experimental results and discussions

5.1. Water filter geometrical analysis

5.1.1. Water treatment filter media elevation analysis

During operation and backwashing, the filter media within the water filter can be dislodged by water flow, reducing media depth. Measuring the media's depth serves as an indicator of the filter media's functional status. Utilizing point cloud data of the water filter, the ground is set as the reference plane to measure the distance between the surface of the filter medium and the ground, as illustrated in Figure 11. Among the six filters analyzed, Filter 2 exhibits the lowest average medium elevation compared to the other five filters as shown in Table 3.

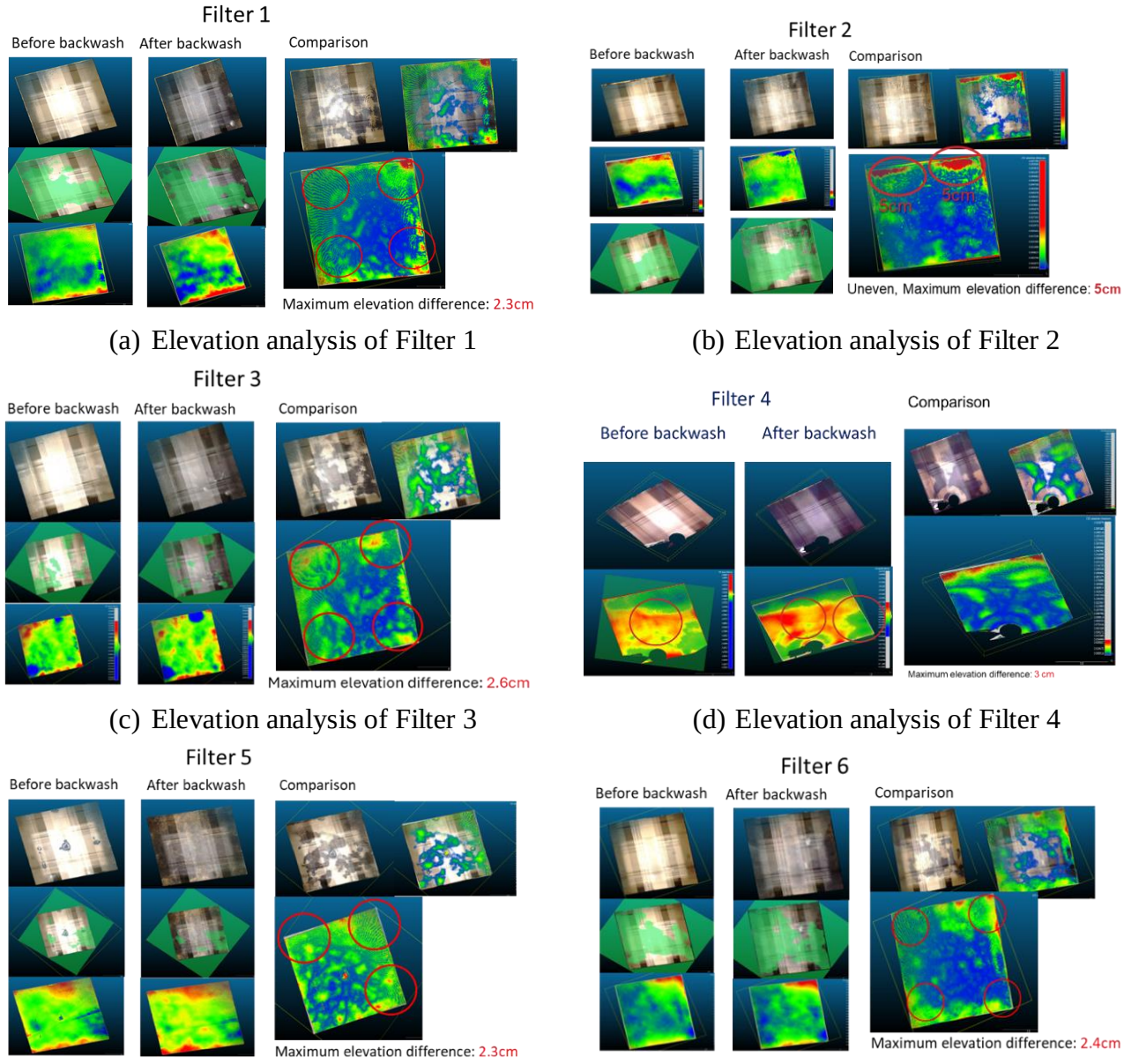

(a) Elevation analysis of Filter 1

(b) Elevation analysis of Filter 2

(c) Elevation analysis of Filter 3

(d) Elevation analysis of Filter 4

(e) Elevation analysis of Filter 5

(f) Elevation analysis of Filter 6

Figure 11. Elevation analysis of the filters.

Table 3. Medium elevation of six filters.

Filter Number	Average Medium Elevation (m)
Filter 1	3.465
Filter 2	3.382
Filter 3	3.395
Filter 4	3.687
Filter 5	3.416
Filter 6	3.371

5.1.2. 3D geometric features analysis of water filter medium surface

We collected surface point cloud data for six water filters before and after backwashing to identify differences between normal and abnormal filter medium surface changes, as shown in Figure 11. Upon comparing the elevation differences of the surfaces pre- and post-backwash, it was observed that the five normal filters exhibited elevation changes exceeding 2 cm. In contrast, Filter 2, identified as abnormal, showed an elevation change of 5 cm.

Furthermore, the geometrical characteristics of the medium surface are repetitive. We double-scanned one normal filter (Filter 3) and one abnormal filter (Filter 2), as shown in Figure 12. For Filter 2, both scans of the medium surface show that the medium bumps up on the same edge with maximum elevation differences of 5 cm and 3.9 cm. However, for Filter 3, both scans show that the medium bumps up on four corners with maximum elevation differences of 2.6 cm and 1.7 cm.

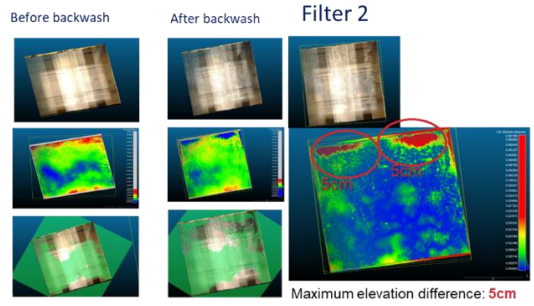

(a) The medium surface of Filter 2 from the first scan

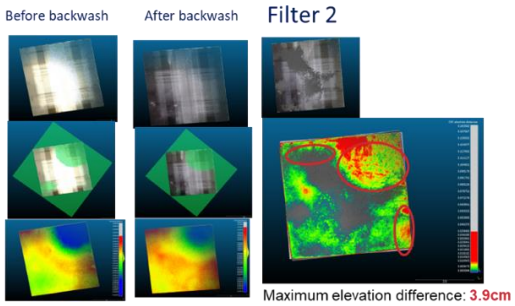

(b) The medium surface of Filter 2 from the second scan

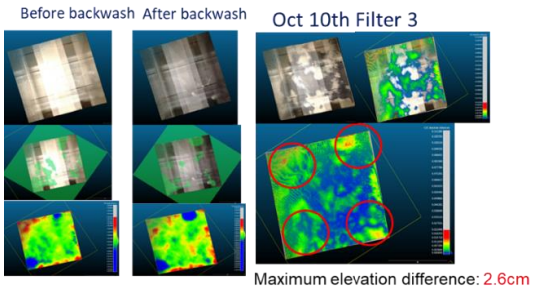

(c) The medium surface of Filter 3 from the second scan

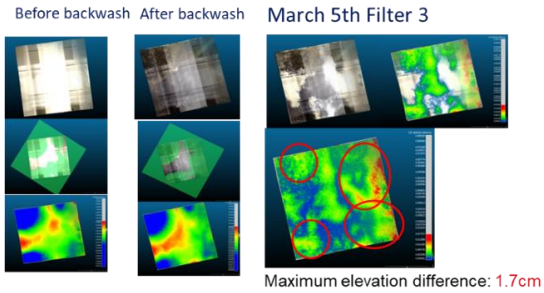

(d) The medium surface of Filter 3 from the second scan

Figure 12. Repeatable geometrical characteristics of the water filter medium surfaces.

Then, four typical geometrical features (roughness, mean curvature, Gaussian curvature, omnivariance) of the point cloud data were selected to quantitatively represent the differences between the abnormal and normal filters, as shown in Figure 13. Due to uneven medium surfaces, the geometrical features of abnormal Filter 2 (roughness: 0.001199788, omnivariance: 0.000209196, mean curvature:

0.320822247, Gaussian curvature: 0.173969705) are higher than those of normal filters (roughness: 0.00082461, omnivariance: 0.000135845, mean curvature: 0.178585816, Gaussian curvature: 0.066004264). However, the planarity of a normal filter (0.942693516) is higher than that of the abnormal filter (0.925826296).

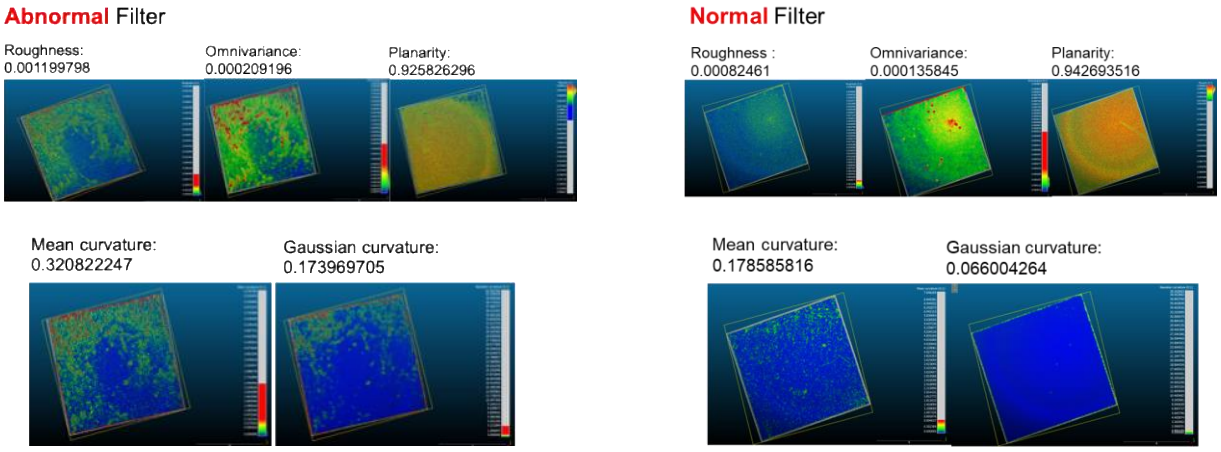

(a) Geometrical features of abnormal filters (b) Geometrical features of normal filters

Figure 13. Geometrical features of filter medium surfaces.

This paper implemented a non-supervised classification technique, specifically K-means, to categorize information elements exhibiting comparable characteristics into unified segments, distinguishing them from elements displaying dissimilar attributes. In the first step, an initial number of clusters was defined. In the second step, each data point was assigned to the closest cluster centroid using the Euclidean distance as the metric, aiming to minimize the within-cluster sum of squares (WCSS). In the next step, the cluster centroids' positions were updated. Steps 1 to 3 were repeated until the cluster centroids did not change. Based on the classification results of the chosen dimensional parameters, the second filtration unit was identified as belonging to the anomalous category, as depicted in Figure 14.

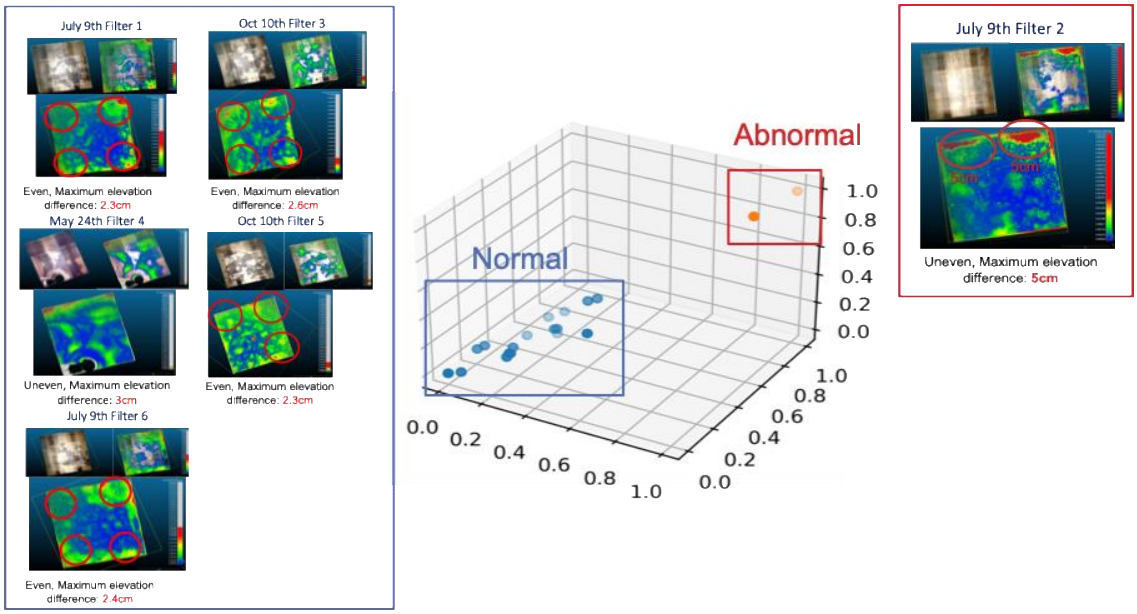

Figure 14. Clustering of geometrical features for abnormal filter detection.

5.1.3. Analysis of 3D geometric features of the water filter on the surface

To investigate the condition of the underdrains in abnormal Filter 2, we also scanned the underdrains to measure their flatness, as shown in Figure 15. As depicted in Figure 15(c), the underdrains show no obvious variations. Additionally, discussions with on-site workers revealed that no sand or particles were found blocking the drain holes. Therefore, we assume that defects within Filter 2's medium may exist.

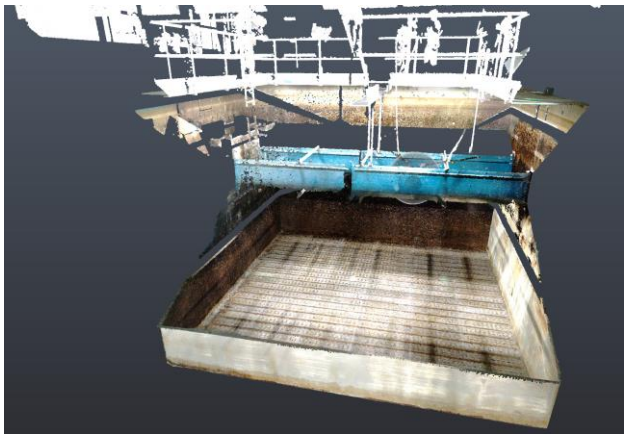

(a) Point cloud of the water filter without medium

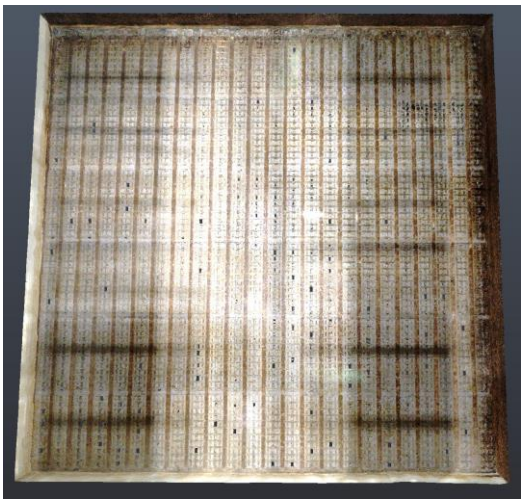

(b) Point cloud of underdrains

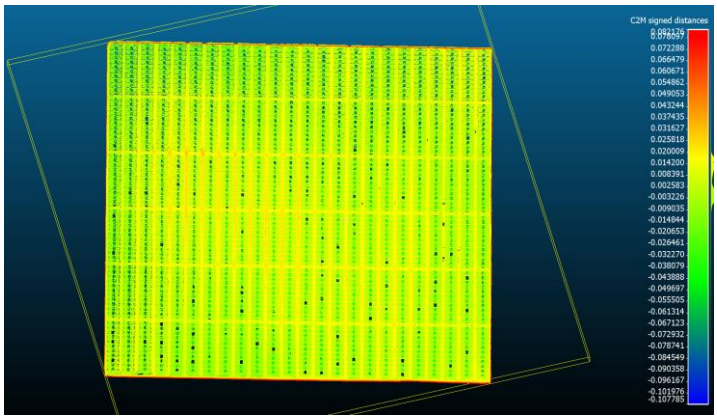

(c) Flatness analysis of the underdrains

Figure 15. Point cloud of the water filter without medium.

5.2. Time-series sensor data analysis

5.2.1. Backwash recovery time and turbidity

We compared the sensor data of six filters at the Shenango Water Treatment Plant from January to October 15, 2019–2021. As shown in Figure 16, there were eight backwash events on these dates. The average duration of Filter 2's backwash is 133.38 minutes across these eight events. For Filter 1 and Filter 6, insufficient data renders the results not statistically significant.

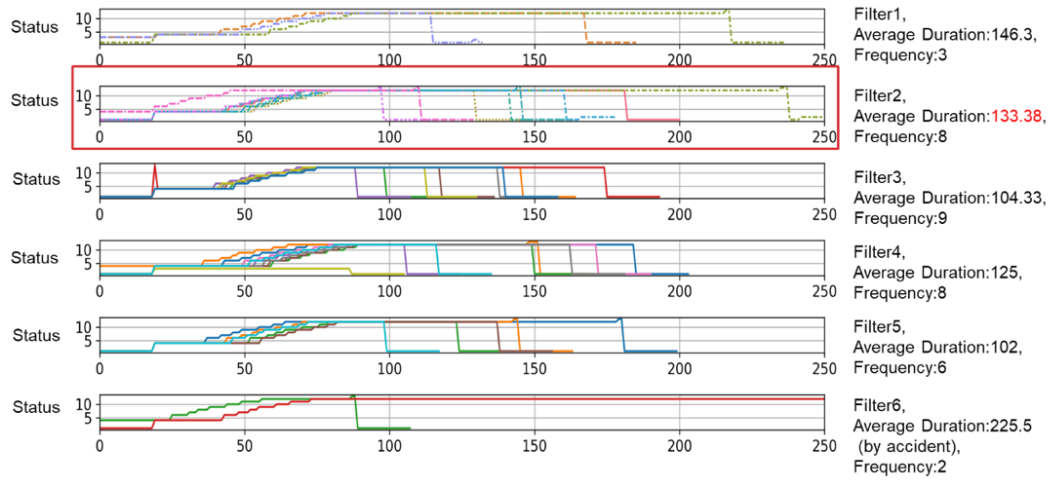

Figure 16. Backwash recovery time (min) analysis of six filters.

Turbidity is a significant parameter for measuring particulate matter levels in water. A crack or break in the filter media allows particulate matter to pass through, rapidly increasing effluent turbidity. A defective underdrain system causes ineffective backwash, creating "dead zones" that lead to turbidity exceedance or breakthrough. As shown in Figure 17, the average turbidity of Filter 2 during eight backwashes is 0.137 NTU, which is higher than that of other filters. Additionally, the 50% and 75% turbidity values of Filter 2 are higher than those of the other five filters, as presented in Table 4.

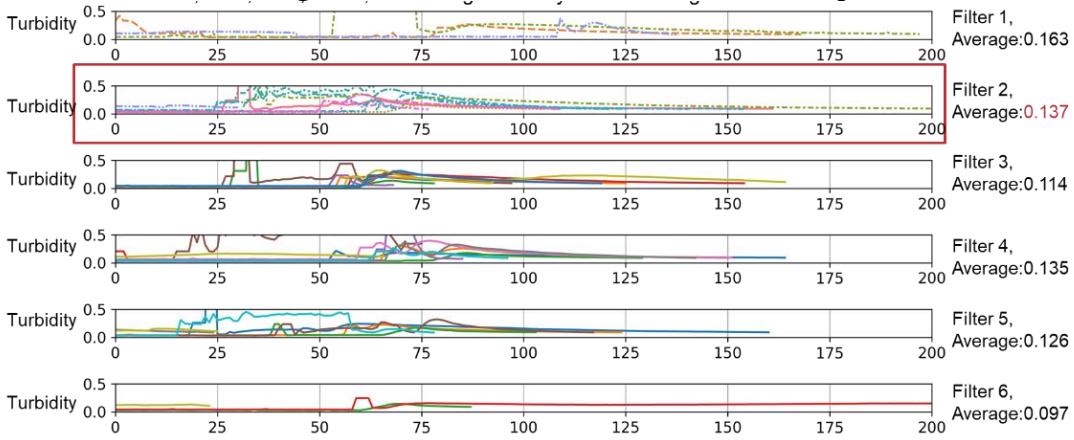

Figure 17. Average backwash turbidity (NTU) analysis of six filters.

Table 4. Average turbidity (NTU) of six filters on 1/15, 4/15, 7/15, and 10/15 from 2019 to 2021.

	Filter1	Filter2	Filter3	Filter4	Filter5	Filter6
50% turbidity	0.0473	0.05406	0.049055	0.05156	0.05417	0.04747
75% turbidity	0.05568	0.059268	0.053858	0.056678	0.056209	0.053293

5.2.2. Water filter production analysis

Filtration unit output capacity is defined as the volume of processed liquid that can be generated prior to necessitating a cleansing cycle. Our assessment methodology incorporated both mean and cumulative throughput measurements to determine the operational efficiency of the filtration mechanisms. As illustrated in Table 5 and Figure 18, the second filtration unit exhibited the highest frequency of

maintenance cycles (190 minutes) while simultaneously demonstrating the most limited mean output capacity (2.96 million gallons). According to backwash times each month, Filter 2 in November and December had more frequent backwashes than the other five filters, especially in December 2021 as shown in Figure 19.

Table 5. Production and backwash times of six filters in 2021 (million gallons).

Filter	Backwash Times (minutes)	Average Production (million gallons)	Total Production (million gallons)
1	181	3.17	574.31
2 (abnormal)	**190**	**2.96**	**561.89**
3	179	3.26	583.70
4	164	3.56	584.46
5	172	3.41	585.80
6	168	3.43	576.44

Figure 18. Productions and related backwash times of six filters in 2021.

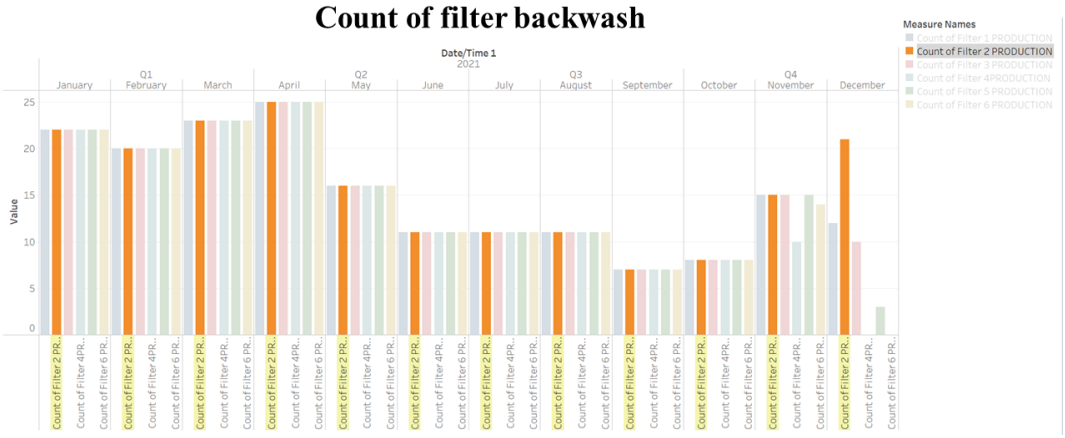

Figure 19. Counts of filter backwash.

We also compared the counts of filter backwash and figured out that Filter 2 had the largest number of backwash as shown in Figure 19. Furthermore, Filter 2 produced less water from January to September 2022 with consistent backwash times, as shown in Figure 20. However, in September, October, and November 2021, Filter 2 had higher production during each backwash, as depicted in Figures 20 and 21. We need to discuss these observations with on-site operators to understand the underlying reasons.

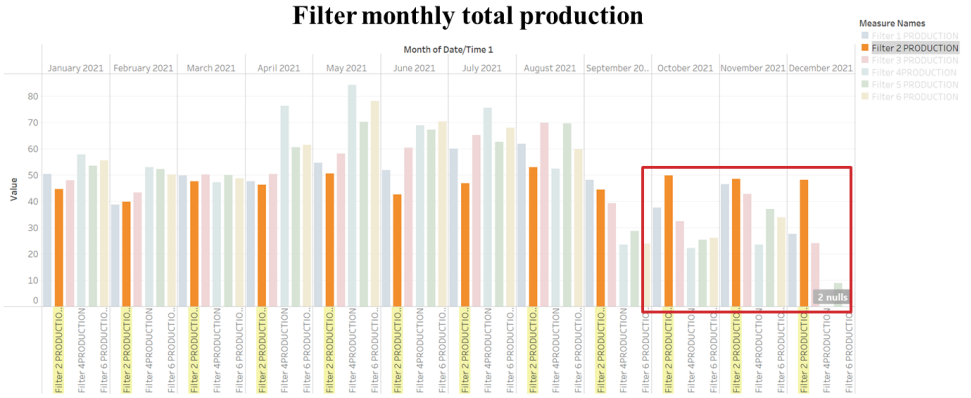

Figure 20. Total monthly filter production.

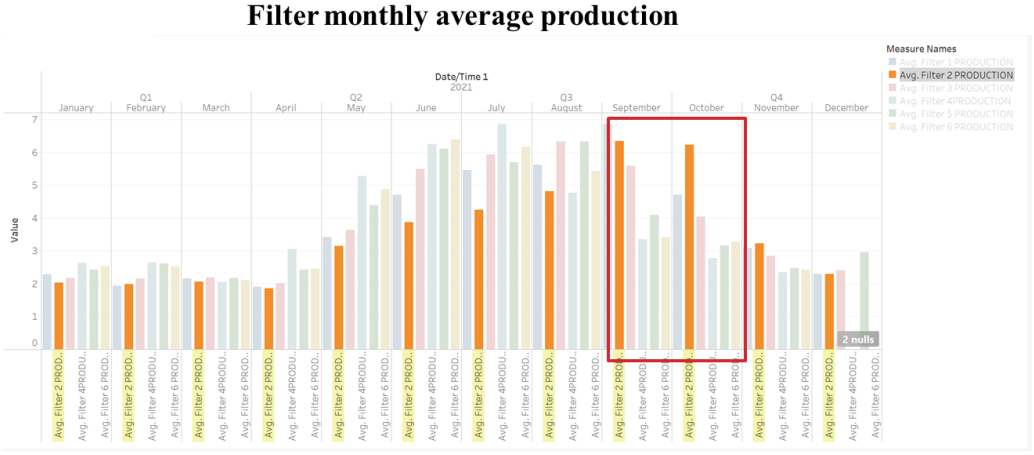

Figure 21. Filter monthly average production.

5.3. Discussion and cost comparison

The geometrical analysis revealed that Filter 2 has higher surface elevations—as bulges on one side of the filter surface—compared to the other five filters. K-means clustering of the geometrical features also identified Filter 2 as an outlier. Filter 2 demonstrated a lower average production between each backwash event and higher average turbidity relative to the other filters in the sensor data domain. These observations collectively indicate that Filter 2 is the abnormal filter among the six filters analyzed.

Uneven backwash flow distribution emerges as the primary factor contributing to the irregular variations in the geometric features of the filter surface. Several potential causes for this uneven flow distribution during backwash include: (1) Blocked Underdrains: Obstructions in the underdrains can disrupt the uniformity of water flow; (2) Mud Balls or Non-Uniformity in the Filter Medium: Inconsistencies in the filter medium or the presence of mud balls can impede water flow.

To investigate these potential causes and validate our hypothesis, we conducted the following examinations: (1) Double-scanning the same filter: This process was intended to identify repetitive uneven surface patterns. (2) Emptying the filter media and inspecting under-drained water pipes: This step aims to detect any blockages or structural defects within the underdrain systems.

Upon double-scanning, we examined both Filter 3 (a normal filter) and Filter 2 (an abnormal filter), as illustrated in Figure 14. The scans of Filter 2 consistently revealed medium bulges on the same edge, with maximum elevation differences of 5 cm and 3.9 cm across the two scans. In contrast, Filter 3 exhibited medium bulges at four corners, with maximum elevation differences of 2.6 cm and 1.7 cm in its two scans. This repetitive pattern in Filter 2 underscores the likelihood of a systematic defect affecting its surface geometry.

Inspection of the filter media and under-drained water pipes, as shown in Figure 15, indicated no apparent variations in the underflows. Discussions with on-site workers confirmed that there were no sand or particle blockages in the drain holes. Consequently, we infer that defects within Filter 2's medium are responsible for the observed geometric irregularities.

To further understand the impact of these defects, we conducted Computational Fluid Dynamics (CFD) simulations, presented in Figure 22. The simulations modeled scenarios where mudballs or dead zones are present within the filter medium. The results indicate that such defects disrupt the uniform flows from the underdrains, causing the water flow velocities across the filter surface to become non-uniform. This non-uniform distribution of flow velocities likely contributes to the uneven geometric changes observed in Filter 2.

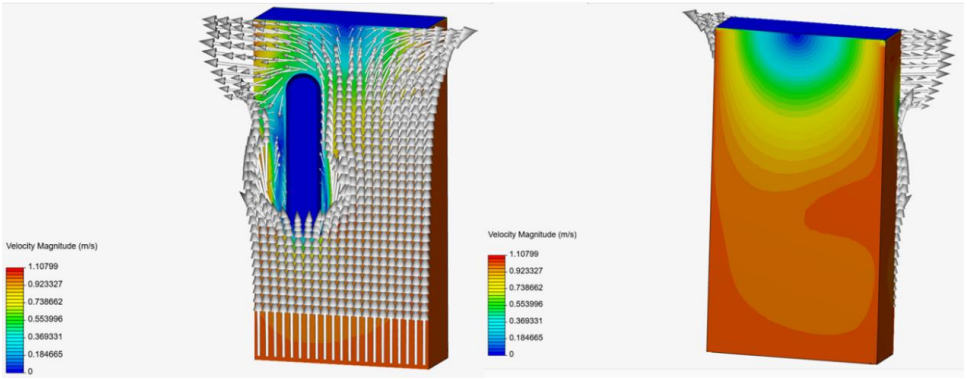

Figure 22. CFD simulation of the water filter backwash with uneven medium.

In summary, the combination of higher surface elevations, classification as an outlier through clustering, reduced production, and increased turbidity in Filter 2, alongside the CFD simulation results—supports the conclusion that uneven backwash flow distribution, caused by defects in the filter medium, is the primary factor leading to its anomalous performance.

Our 3D scanning methodology offers significant cost savings compared to traditional filter inspections. Traditional methods require 4–6 hours with two operators per filter, while our approach needs < 1 hour with one operator, reducing labor costs from $3,000 to $300 for a six-filter inspection. Downtime decreases from 6–8 hours to < 2 hours per filter, saving approximately $7,200 in production value for a typical 10 MGD plant.

Early defect detection provides additional benefits, as demonstrated when we identified Filter 2's issues early. This allowed targeted repairs costing $2,500 instead of a $12,000 underdrain replacement. Assuming one major failure prevention every three years, this represents annual savings of $3,167. Overall, our methodology can save water treatment facilities approximately $11,900 annually through combined reductions in labor, downtime, and maintenance costs.

5.4. Limitations and practical considerations

While the proposed methodology demonstrates promise for non-invasive filter assessment, several limitations warrant discussion. Regarding time efficiency, our approach requires 5–10 hours per filter (including draining, scanning, and data processing), which represents a 50%–60% reduction in downtime compared to traditional manual inspections that typically require 1–2 days per filter. However, the initial equipment setup and analyst training present additional overhead costs that must be considered when implementing this technology at scale. The validation of root causes without invasive techniques presents another significant challenge. We mitigated this limitation through multiple complementary approaches: correlation with sensor data (Section 5.2), computational fluid dynamics simulations (Figure 22), verification through repeated scanning (Figure 12), and limited invasive verification of the underdrains in Filter 2 (Figure 15). These methods collectively strengthened our confidence in the findings, although they provide indirect rather than direct confirmation of specific defects.

Our methodology's reliability was assessed through multiple approaches. The 3D laser scanner (FARO Focus) provides ± 1 mm accuracy at 10 m distance with proper calibration. Scans were performed during non-operational hours to minimize environmental interference. Repeated scans of Filters 2 and 3 (Figure 12) confirmed measurement repeatability, with maximum elevation differences of ≤ 5 cm for abnormal filters and ≤ 2.6 cm for normal filters. Geometric features were derived from covariance matrix eigenvalues (Equations (1) and (2)), with K-means clustering and silhouette analysis validating cluster separation (Figure 14). Filter 2's classification as an outlier remained consistent across 95% of 100 randomized initializations. CFD simulations (Figure 22) further confirmed that surface irregularities correlate with subsurface flow disruptions.

Our 3D scanning methodology offers significant cost savings compared to traditional filter inspections. Traditional methods require 4–6 hours with two operators per filter, while our approach needs < 1 hour with one operator, reducing labor costs from $500 to $50 for a single filter inspection. Downtime decreases from 6–8 hours to < 2 hours per filter, saving approximately $1,200 in production value for a typical 10 MGD plant. Early defect detection provides additional benefits, as demonstrated when we identified Filter 2's issues early. This allowed targeted repairs costing $2,500 instead of a

$12,000 underdrain replacement. Assuming one major failure prevention every three years, this represents annual savings of $3,167. Overall, our methodology can save water treatment facilities approximately $8,317 annually through combined reductions in labor, downtime, and maintenance costs, as shown in Table 6.

Table 6. Long-term operational savings.

Cost Category	Traditional Method	Proposed Method	Annual Savings
Labor (per filter)	$500	$50	$450
Downtime (per filter)	$1,600	$400	$1,200
Preventive Maintenance	$5,000	$1,500	$3,500
Emergency Repairs (annualized)	$4,000	$833	$3,167
Total Annual Cost	$11,100	$2,783	$8,317

Our findings provide practical insights for enhancing water filter design and durability. Surface irregularities strongly correlate with subsurface defects (Section 5.1.2), suggesting that integrating 3D LiDAR sensors into filter structures could enable continuous monitoring and proactive maintenance. CFD simulations (Figure 22) showed that uneven gravel layers create backwash flow dead zones. Future designs could use graded orifice sizes or adaptive flow controllers to maintain consistent flow distribution despite minor subsurface misalignments. Media displacement observations (Section 5.3) indicate the need for more stable gravel beds. A multi-layered gradation with smaller, uniform gravel in upper layers and anti-fluidization mesh could reduce sand migration and mud ball formation. Finally, incorporating removable access panels or transparent sections in filter walls would simplify non-invasive inspections, while standardized baseline surface profiles would streamline defect detection, allowing more frequent assessments without operational disruptions.

Our analysis of the AQUA water treatment plant's backwash protocol reveals that current parameters (15-minute air scour, 5,000 gpm initial backwash, 14,000 gpm for 6 minutes, followed by 5,000 gpm for 3 minutes) are based primarily on operational experience rather than real-time filter conditions. The 3D surface analysis demonstrated significant variations in media bed conditions between filters with similar operational histories, suggesting that standardized backwash parameters are suboptimal for addressing variable fouling patterns.

The geometric feature analysis indicated that backwash rates should be dynamically adjusted based on actual filter conditions rather than fixed durations or turbidity thresholds. We recommend implementing an adaptive control system that monitors filter surface geometry and adjusts backwash parameters, accordingly, including variable air scour duration, dynamic high-rate backwash periods, and adjustable filter-to-waste periods based on actual ripening profiles. This approach would optimize water usage, reduce energy consumption, and extend filter run times by providing customized cleaning specific to each filter's current condition.

Several inherent technical limitations persist: (1) The laser scanning technique cannot detect defects beneath dense filtration media exceeding certain thickness thresholds; (2) The approach requires baseline data of normal filter operation for comparison, which may not be available for all facilities; and (3) Environmental factors such as humidity and ambient lighting can affect scan quality, necessitating controlled conditions. Furthermore, different types of defects may produce similar surface patterns, creating potential ambiguity in diagnosis, while deeply buried defects might manifest as subtle surface irregularities that fall below detection thresholds. Our approach currently functions most effectively

as a comparative analysis tool among similar filters rather than as an absolute diagnostic method. Future work should focus on developing a comprehensive defect library by correlating known defects (verified through invasive inspection) with their surface manifestations, thereby improving diagnostic specificity for various filter configurations and operational conditions.

6. Conclusion and future research

In this study, we tested the hypothesis that uneven washing processes—resulting from inconsistent gravel support and defective backwash pipes—lead to irregular 3D geometric changes on the filter surface and abnormal sensor data. This research contributes to the early detection of defective filters, thereby preventing costly repairs to damaged or malfunctioning water filter components. We collected 3D point cloud data through laser scanning and time-series sensor data from water treatment plants, including six filters before and after backwashing, to analyze and diagnose the structural integrity of water treatment plant filters and identify potential backwash issues. We proposed geometric features from the filter media's surface point clouds and used the clustering method capable of reliably predicting geometric defects in water filters based on surface shape changes and related geometric features. Additionally, we defined key performance indexes to evaluate the filters, such as water turbidity and production, using time-series sensor data from water treatment plants to evaluate the performance of the water filters. The proposed method was validated using the collected data, successfully identifying defective filter (Filter 2) and analyzing the underlying causes of their malfunction. This paper demonstrates the effectiveness of combining 3D geometric analysis with sensor data for fault detection in water treatment systems. For future research, we plan to collect point cloud and sensor data from additional water treatment plants to enhance the applicability and robustness of the provided method. Expanding the dataset will allow us to refine the proposed model and ensure its effectiveness across diverse operational environments. Additionally, integrating real-time monitoring systems could further improve the predictive capabilities and responsiveness of the fault detection framework.

Acknowledgments

The authors acknowledge the funding agency for this study. Pennsylvania Infrastructure Technology Alliance and AQUA America sponsor the research.

Conflicts of interests

The authors declare no conflict of interest.

Authors' contribution

Pengkun Liu: investigation, methodology, visualization, validation, writing—original draft. Jinhua Xiao: investigation, supervision, review & editing. Pingbo Tang: conceptualization, supervision, writing—review & editing, funding acquisition.

References

[1] Yu P, Cao J, Jegatheesan V, Shu L. Activated sludge process faults diagnosis based on an improved particle filter algorithm. *Process Saf. Environ. Prot.* 2019, 127:66–72.

[2] Longo S, d'Antoni BM, Bongards M, Chaparro A, Cronrath A, *et al.* Monitoring and diagnosis of energy consumption in wastewater treatment plants. A state of the art and proposals for improvement. *Appl. Energy* 2016, 179:1251–1268.

[3] McGlohorn G, By E, Trofatter G, Kinard D, Randolph PB, *et al.* Filter assessment manual. 2003, pp. 2–3. Available: https://awopnews.wordpress.com/wp-content/uploads/2014/06/filter-assessment-manual-dec2003.pdf (accessed on 20 May 2025).

[4] Piri I, Homayoonnezhad I, Amirian P. Investigation on optimization of conventional drinking water treatment plant. In *2010 2nd International Conference on Chemical, Biological and Environmental Engineering*, Cairo, Egypt, November 2–4, 2010, pp. 304–310.

[5] Onyango LA, Quinn C, Tng KH, Wood JG, Leslie G. A study of failure events in drinking water systems as a basis for comparison and evaluation of the efficacy of potable reuse schemes. *Environ. Health Insights* 2015, 9:EHI-S31749.

[6] Jameson PB, Hung YT, Kuo CY, Bosela PA. Cryptosporidium outbreak (water treatment failure): North Battleford, Saskatchewan, Spring 2001. *J. Perform. Constr. Facil.* 2008, 22(5):342–347.

[7] Passantino L, Rhoades J. How are my filters doing? Filter profiling reveals all. 2014, pp. 4–5. Available: https://cdn.ymaws.com/www.azwater.org/resource/group/25c2bfe3-42d4-4cd3-9149-4911c8416e5e/Downloads/2014-02-18_Seminar/Session_01.pdf (accessed on 20 May 2025).

[8] Nix DK, Taylor JS. *Filter evaluation procedures for granular media*, 2nd ed. Denver: American Water Works Association, 2018.

[9] Bosché F, Biotteau B. Terrestrial laser scanning and continuous wavelet transform for controlling surface flatness in construction–a first investigation. *Adv. Eng. Inf.* 2015, 29(3):591–601.

[10] Bosché F, Guenet E. Automating surface flatness control using terrestrial laser scanning and building information models. *Autom. Constr.* 2014, 44:212–226.

[11] Puri N, Valero E, Turkan Y, Bosché F. Assessment of compliance of dimensional tolerances in concrete slabs using TLS data and the 2D continuous wavelet transform. *Autom. Constr.* 2018, 94:62–72.

[12] Wang Q, Kim MK, Sohn H, Cheng JC. Surface flatness and distortion inspection of precast concrete elements using laser scanning technology. *Smart Struct. Syst.* 2016, 18(3):601–623.

[13] Liu J, Li D, Feng L, Liu P, Wu W. Towards automatic segmentation and recognition of multiple precast concrete elements in outdoor laser scan data. *Remote Sens.* 2019, 11(11):1383.

[14] Li D, Liu J, Feng L, Zhou Y, Liu P, *et al.* Terrestrial laser scanning assisted flatness quality assessment for two different types of concrete surfaces. *Measurement* 2020, 154:107436.

[15] Erdélyi J, Kyrinovič P, Lipták I, Funtík T. Diagnostics of areation tank of wasteeater treatment plant using terrestrial laser scanning. In *International Multidisciplinary Scientific GeoConference: SGEM*, Albena, Bulgaria, June 30 to July 6, 2016, pp. 223–230.

[16] Yu P, Wu H, Liu C, Xu Z. Water leakage diagnosis in metro tunnels by intergration of laser point cloud and infrared thermal imaging. In *ISPRS-International Archives of the Photogrammetry, Remote Sensing and Spatial Information Sciences*, Beijing, China, May 7–10, 2018, pp. 2167–2171.

[17] Moritani R, Kanai S, Date H, Watanabe M, Nakano T, *et al.* Cylinder-based efficient and robust registration and model fitting of laser-scanned point clouds for as-built modeling of piping systems. *Comput. Aided Des. Appl.* 2019, 16:396–412.

[18] Marzouk M, Ahmed R. BIM-based facility management for water treatment plants using laser scanning. *Water Pract. Technol.* 2019, 14(2):325–330.

[19] Yang Y, Yang N, Li L, Gao F. Defect diagnosis technology based on multi-spectral point cloud. In *2021 IEEE Electrical Insulation Conference (EIC)*, Denver, USA, June 7–28, 2021, pp. 643–646.

[20] Chethana B, Patil AK, Chai YH. Development of an efficient pipeline retrofitting application for a water treatment facility. In *2018 IEEE International Conference on Consumer Electronics-Asia (ICCE-Asia)*, JeJu, Korea, June 24–26, pp. 206–212.

[21] Catalin G, Neamțu C, Comes R, Hurgoiu D. Analyzing the accuracy of 3D models generated using photogrammetry compared to terrestrial laser scanning. Case study of a water treatment plant layout. *Acta Tech. Napocensis, Ser. Appl. Math. Mech. Eng.* 2021, 64(4).

[22] Faruk DÖ. A hybrid neural network and ARIMA model for water quality time series prediction. *Eng. Appl. Artif. Intell.* 2010, 23(4):586–594.

[23] Liu J, Li Q, Yang H, Han Y, Jiang S, *et al.* Sequence fault diagnosis for PEMFC water management subsystem using deep learning with t-SNE. *IEEE Access* 2019, 7:92009–92019.

[24] Liu S, Xu L, Li Q, Zhao X, Li D. Fault diagnosis of water quality monitoring devices based on multiclass support vector machines and rule-based decision trees. *IEEE Access* 2018, 6:22184–22195.

[25] Li D, Chen D, Goh J, Ng SK. Anomaly detection with generative adversarial networks for multivariate time series. *arXiv* 2018, arXiv:1809.04758.

[26] Wang P, Zhang J, Wan J, Wu S. A fault diagnosis method for small pressurized water reactors based on long short-term memory networks. *Energy* 2022, 239:122298.

[27] Ghoneim SS, Taha IB. A new approach of DGA interpretation technique for transformer fault diagnosis. *Int. J. Electr. Power Energy Syst.* 2016, 81:265–274.

[28] Chen G, Liu M, Chen J. Frequency-temporal-logic-based bearing fault diagnosis and fault interpretation using Bayesian optimization with Bayesian neural networks. *Mech. Syst. Signal Process.* 2020, 145:106951.

[29] Liu J, Li G, Liu B, Li K, Chen H. Knowledge discovery of data-driven-based fault diagnostics for building energy systems: a case study of the building variable refrigerant flow system. *Energy* 2019, 174:873–885.

[30] Mayr A, Rutzinger M, Bremer M, Oude Elberink S, Stumpf F, *et al.* Object-based classification of terrestrial laser scanning point clouds for landslide monitoring. *Photogramm. Rec.* 2017, 32(160):377–397.

[31] Guo L, Chehata N, Mallet C, Boukir S. Relevance of airborne lidar and multispectral image data for urban scene classification using Random Forests. *ISPRS J. Photogramm. Remote Sens.* 2011, 66(1):56–66.

[32] Hackel T, Wegner JD, Schindler K. Contour detection in unstructured 3D point clouds. In *Proceedings of the IEEE Conference on Computer Vision and Pattern Recognition (CVPR)*, Las Vegas, USA, June 27–30, 2016, pp. 1610–1618.

[33] Weinmann M, Jutzi B, Mallet C. Feature relevance assessment for the semantic interpretation of 3D point cloud data. *ISPRS Ann. Photogramm. Remote Sens. Spatial Inf. Sci.* 2013, 2:313–318.

[34] McGregor S. Know your filters. In *64th Annual Water Industry Engineers and Operators' Conference*, Bendigo, Australia, September 5–6, 2001, pp. 11–17.